



Kinematic process and mechanism of the two slope failures at Baige Village in the upper reaches of the Jinsha River, China

Fei Chen^{1,2} · Yunjian Gao³ · Siyuan Zhao³ · Jianhui Deng³  · Zongliang Li⁴ · Renji Ba⁴ · Zhiqiu Yu³ · Zhongkang Yang³ · Sai Wang³

Received: 13 May 2020 / Accepted: 12 February 2021 / Published online: 23 February 2021
© Springer-Verlag GmbH Germany, part of Springer Nature 2021

Abstract

On Oct. 10 and Nov. 3, 2018, two landslides, i.e., the “10.10” and “11.3” rockslides, occurred successively at Baige Village, Jiangda County, Tibetan Autonomous Region, P. R. China. The two landslides are located in the upper reaches of the Jinsha River and both dammed the river. Immediately since the slides, the authors have been working on the slides and help disaster reduction. Based on the data collected by April 2020, this paper is aimed at clarifying the geological condition of the slides and at explaining why the slides occurred and what the whole sliding process was. Conclusions are summarized as follows. First, the two landslides occurred in the suture belt of the Jinsha River and the rocks are composed of tectonic *mélange* slices of mainly gneiss intermingled with carboniferous slate and marble and with intruded serpentine and granite porphyry. The gneiss generally bears a schistosity plane with an averaged attitude of N47° W/47°, dipping into the slope. Secondly, long-term geomorphological evolution of the bank slope due to river incision contributed to the progressive slope deformation for the development of the “10.10” rockslide. No preferential joints exist in the slope, but alteration and weathering played important roles in its occurrences. Rainfall and earthquakes may also accelerate its deformation. Thirdly, the “10.10” rockslide is of high-speed wedge-like slope failure with a high-position and a high-shear outlet. Its sliding and deposition process demonstrate special features as initial speed, collision between debris, surging waterjet, and second slipping. Fourthly, the whole process of the “10.10” rockslide can be divided into 6 steps, i.e., startup of the major sliding and sliding resistance zones, sliding initiation of the trailing zone, formation of debris-eroded zones, collision of debris and triggering waterjet and mist, secondary slip of the landslide dam, and surface flush in the deposition area. The estimated speed may reach as high as 67 m/s. Fifthly, the “11.3” rockslide follows a different mode, i.e., wedge cleaving effect. And finally, the cracked zones still have the risk to constitute a potential landslide and to dam the river again.

Keywords Baige landslide · Mechanism · Kinematic process · Landslide dam · Initial speed · Waterjet erosion

Introduction

The West Sichuan province is located on the southeast brim of the Tibetan Plateau and is characterized by sharp relief change, deep valley, and strong earthquakes. Four major rivers are developed in the area, i.e., the Min, Dadu, Yalong, and Jinsha Rivers (Fig. 1). The Jinsha River is the major one, and the other three can be taken as its tributaries, as the Yalong River flows into the Jinsha River at Panzhihua City and the Dadu River flows into the Min River in Leshan City and then joins in the Jinsha River at Yibing City. The Jinsha River is referred to the Changjiang River downstream of Yibing City.

Such high-relief mountainous regions with actively tectonic background developed a great number of historical or pre-historic landslide dams in the four major river catchments, most of which were triggered by seismic events. Dai et al.

✉ Jianhui Deng
jhdeng@scu.edu.cn

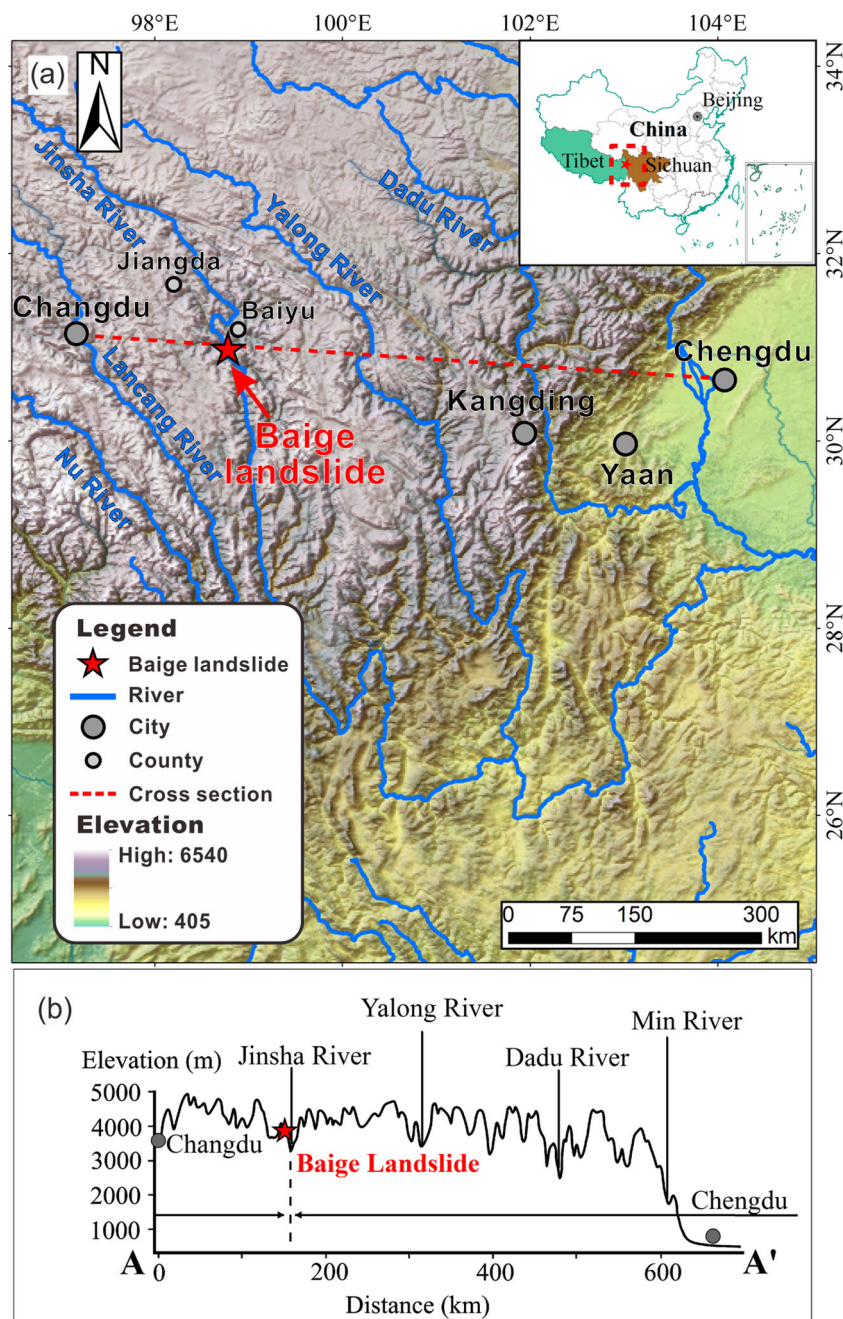
¹ College of Architecture and Environment, Sichuan University, Chengdu 610065, China

² School of Architecture and Civil Engineering, Chengdu University, Chengdu 610106, China

³ State Key Laboratory of Hydraulics and Mountain River Engineering, College of Water Resource and Hydropower, Sichuan University, Chengdu 610065, China

⁴ Chengdu Center of China Geological Survey, Chengdu 610081, China

Fig. 1 Geographical location of the Baige landslides



(2005), Deng et al. (2017), and Wang et al. (2019b) studied the landslide damming events along the Dadu River near Luding County that were triggered by the activity of the Xuanshuihe Fault belt. Wei et al. (2015), Ma et al. (2018), and Zhao et al. (2019) discussed the landslide damming events near Diexi of the Min River, which are associated with the activity of the Huya Fault. Zhang et al. (2011), Chen et al. (2013, 2018, 2019), and Wang et al. (2014) investigated the series landslide damming events in the river segments between Batang County and Benzilan Town of the Upper Jinsha River and concluded that they were induced by the Jinsha River Fault belts. The Only exception is the

Tanggudong landslide damming event of the Yalong River, which was caused by intense rainfall (Chen et al. 1992). However, two successive landslides that occurred at Baige were not directly induced by either earthquake or rainfall on Oct. 10 and Nov. 3, 2018 (named as the “10.10” and “11.3” rockslides), both of which blocked the upper reaches of the Jinsha River and caused severe flood risks for the downstream river catchment. Many efforts have been made on the two slides since their occurrences. Except for a news report by Liang et al. (2019), the other papers focused respectively on topics as dam-breaching flood prediction or modeling (Zhang et al. 2019a; Chen et al. 2020; Fan et al. 2020), slope

deformation history through remote sensing techniques (Fan et al. 2019; Ouyang et al. 2019; Yang et al. 2019; Li et al. 2020a, 2020b; Liu et al. 2020), the monitoring techniques and data during emergency response, and the mechanism and dynamics of the two slides (Zhang et al. 2019b; Li et al. 2019; Wang et al. 2019a; Wu et al. 2019; Tian et al. 2020). Due to the peculiar geological and tectonic background in the area, the specific characteristics of lithology and geological structures were kept unclear that need to be further accounted for; and the mechanisms and kinematic processes of the two slides are still not well clarified. This paper is aimed at characterizing the geomorphological and geological features of the two landslides, at revealing the mechanism and kinematic process of the slides, and at discussing the future impacts of potential failures. The up-to-date status of the slope stability will also be briefly described.

Geological and geo-environmental background

Geo-environmental background

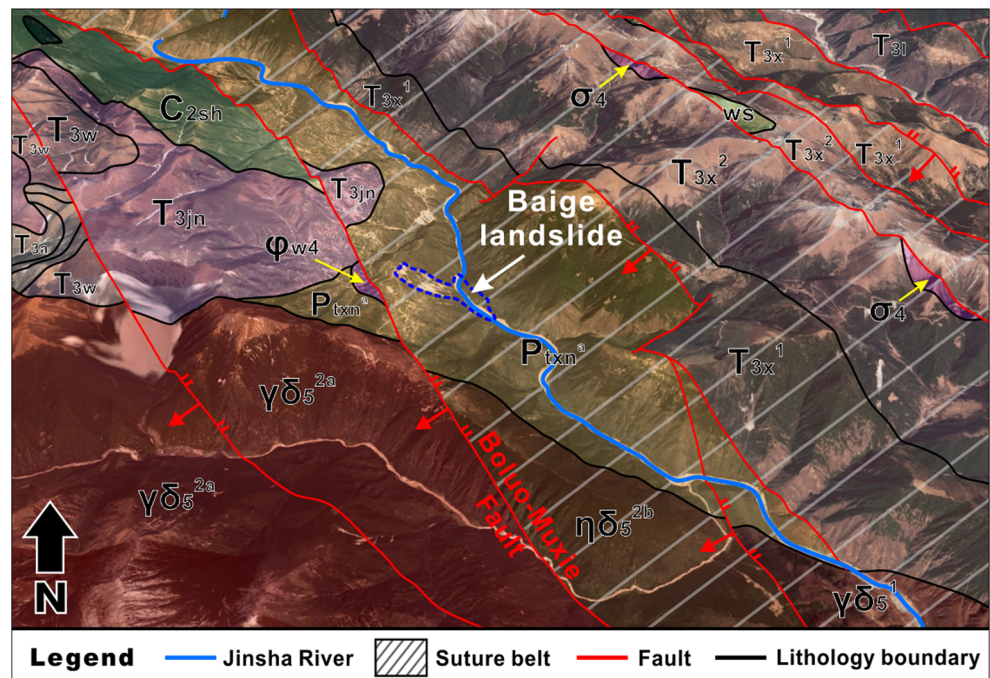
Baige Village is located geographically at $31^{\circ} 4' 30.86''$ N, $98^{\circ} 41' 52.05''$ E (the location of Gongze Monastery), on the right bank of the Jinsha River. It is a small village of Boluo Town, Jiangda County, Tibetan Autonomous Region, China, and can be reached by a simple road named as S201 from Boluo Town before the “10.10” rockslide event. The area is characterized by strongly erosional landform (Fig. 2), where the planation surface of the Tibetan Plateau is between 4000 and 4600 m

above sea level (a.s.l.), and the Jinsha River undercuts the plateau to the current riverbed, forming a V-shaped valley. Baige Village sits at the elevation of 3790m a.s.l., on the southeast slope of a small hill ridge trending $N19^{\circ}$ E. The Jinsha River, the boundary river of Tibetan Autonomous Region and Sichuan Province, flows at the toe of the Baige slope, forming a gentle river bend. The “10.10” rockslide occurred at the crown of the river bend, where the normal water level of the river is about 2880 m a.s.l. The slide is in the reservoir area of Yebatan Hydropower Station being under construction, and their linear distance is ~ 50 km.

The study area is located in the suture belt of the Jinsha River, which was initiated in Hercynian movement and evolved in late Indosinian movement, Yanshan movement, and Himalayan movement. So the tectonic setting of the area is quite complex, faults, and folds are well developed. The major faults in the area generally strike NW-SE, and the Boluo-Muxie Fault is the nearest one to the slides which strikes $N30^{\circ}$ W and dips $50\text{--}70^{\circ}$ to SW. The fault is 146 km long, and its fault belt is 100-300 m wide.

Proterozoic, Carboniferous, and Triassic strata are the major rocks in the study area. The Proterozoic stratum belongs to the Xionsong group (P_{txn}), composed mainly of gneiss (P_{txn}^a) and marble (P_{txn}^b); Carboniferous stratum is clastic rocks and limestone of the Shengpa group (C_{2sh}); and the Triassic strata include sandstone and sandwiched limestone (T_{3jn}), clastic rocks (T_{3x}^1), and limestone (T_{3x}^2). Along the Boluo-Muxie fault and near the slides, ultramafic rock and serpentine (φ_{w4}) of Hercynian Phase are intruded (Fig. 2). Acidic rocks are also intruded, mainly granodiorite ($\gamma\delta_5^{2a}$) of Yanshan Phase in the South. Granite porphyry of possibly

Fig. 2 Landform and geological setting of the Baige area



Yanshan Phase can also be found in local places. The intrusion of the igneous rocks has great influence on the formation of the slides.

The climate in Jiangda County is mildly ranging from -15°C to 28°C with yearly averaged temperature of 4.5°C . Rainfall is quite seasonal, mainly concentrated from June to September, and the annually averaged rainfall is 549.0 mm. In Sep. 2018, the monthly rainfall is 103.2 mm, a little more than the regular level; however, no rainfall is recorded before the landslide.

The design earthquake intensity in the area is VII. The latest seismic record suggests a large earthquake occurred at 5:23, Aug. 12, 2013, with a magnitude of 6.1 on the Richter scale. Its epicenter is at $\text{N}30.0^{\circ}$ and $\text{E}98.0^{\circ}$, ~ 140 km away from the slides. No appreciable seismic events are ever recorded before the slides. In summary, no evidence indicates the slides were immediately triggered by a rainfall or seismic event.

Geology and geomorphology of the slides

The two slides are located within 1 km to the Northeast of Baige Village and the geographical location of their main scarps is around $98^{\circ} 41' 52.30'' \text{E}$, $31^{\circ} 4' 55.12'' \text{N}$, quite near the hill ridge and the Road S201, where the elevation is at 3720 m a.s.l. (Fig. 3). The bank slope, where the slides developed, has an average slope angle of 33° , while its upstream slope is steeper (36°) and the downstream slope is gentler (29°). Three platforms (PF1, PF2, and PF3) with a relatively gentle slope are developed on the hillslope before the 2018 land sliding (Fig. 3). The upper PF1 developed most extensively in an area with an elevation of 3450–3550 m a.s.l.; the middle PF2 is relatively smaller with an elevation of 3100–3200 m a.s.l.; and the lower PF3 is the smallest with an elevation of 2940–2970 m a.s.l. Two small gullies (GL1 and GL2) developed on the hillslope. The upstream GL1 has a flowrate of around 1 liter every minute in all seasons. The water is mainly from a spring at the elevation of 3550 m a.s.l. below the road S201. The downstream GL2 has water only when it rains. The gullies are generally parallel and run down the slope along its dip direction of $\text{N}67^{\circ} \text{E}$, suggesting that the three platforms were formed by hillslope erosion during long-term river incision. To the further south, there exists a large gully named GL3 and an alluvium fan is well developed at the gully mouth.

Bedrock in the sliding area is mainly gneiss of the Xionsong group (Ptxn^a). However, due to the periodically tectonic movements of the Jinsha River suture belt, the gneiss is separated into *mélange* slices (Fig. 4a). Blocks of carbonaceous slate and marble exist locally and are in contact with gneiss by small faults (Fig. 4b). Serpentine and granite porphyry can also be found in the sliding area (Fig. 4c).

Even though the tectonic background, the gneiss generally bears schistosity plane with an averaged attitude of $\text{N}47^{\circ} \text{W}/47^{\circ}$, that is, dipping into the slope (Fig. 5). In accordance

with the three platforms, three lithology zones can also be conceptually divided for the slope in terms of the extent of weathering and alteration. Zone 1 is above the elevation of platform PF1, and its rocks are adversely affected by the intrusion of the ultramafic rock and serpentine ($\varphi_{\omega 4}$), and are heavily serpentinized and completely weathered. Zone 2 is between PF1 and PF2, consisting of heavily weathered rock; and Zone 3 is located below PF2, and its rock consists mainly of moderately weathered gneiss (Fig. 5). The dip angle of schistosity planes reduces gradually from Zone 3 to Zone 1; the angle reaches as steep as 58° in Zone 3 but as gentle as 15° in Zone 1, suggesting toppling deformation of the strata.

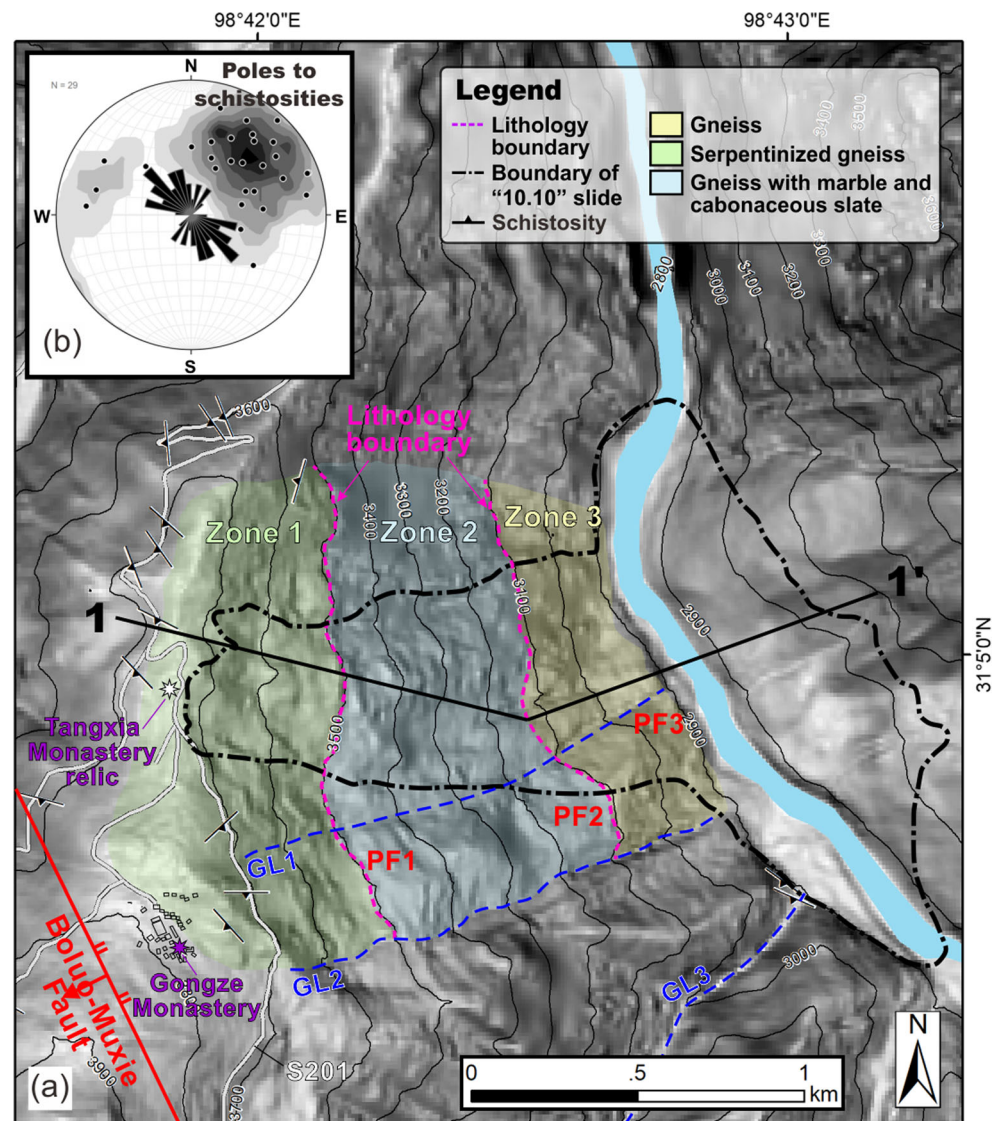
Except the gneiss, other rocks are distributed quite locally. Serpentine is mainly located around the left portion of the main scarp of the slides and is completely weathered (Fig. 4c); granite porphyry appears as dykes along the schistosity planes of the gneiss mainly at the left (Northern) boundary of the slides, and its thickness varies from tens of centimeters to a few meters. It can also be found in the fractured rock at the right portion of the main scarp, and the thickness is only tens of centimeters. Granite porphyry is not metamorphosed or altered, but moderately weathered, suggesting that it was most likely to be intruded in the Yanshan Phase; carbonaceous slate is concentrated at the platform PF1 at the right (Southern) boundary, and small slices can also be found in other parts in Zones 2 and 3; marble can only be occasionally found in the source area; however, it is quite common beyond the right boundary and below the platform PF1.

The lithological setting indicates that the rock mass quality in the sliding area is poorer than those both in the upstream slope and the downstream slope, which may explain why the “10.10” rockslide occurred at exactly the place. As to rock mass quality, the Zone 3 is composed of rocks with comparatively strong strength and is resistant to a slope failure; Zone 2 is weaker compared to the lower portion; and the rock in Zone 1 is the weakest and is favorable to a sliding. Attitudes of 27 schistosity planes were measured during field investigation (Fig. 3b). Except for the schistosity plane, no preferential joint is well developed.

“10.10” rockslide

The exact time of the first slide is at 22:05:36 (Beijing time, UTC+8) on Oct. 10, 2018, based on the interpretation of slide-induced seismograms (Zhang et al. 2019b). The geomorphological characteristics of the “10.10” rockslide was interpreted on the orthograph taken by Unmanned Aerial Vehicle (UAV) on Oct. 12, 2018 (Fig. 6). Two areas, i.e., source area and deposition area, and a number of zones were identified so as to facilitate the description of failure mechanism and movement.

Fig. 3 Geomorphology and geology of the Baige hillslope before the 2018 landslides



Source area

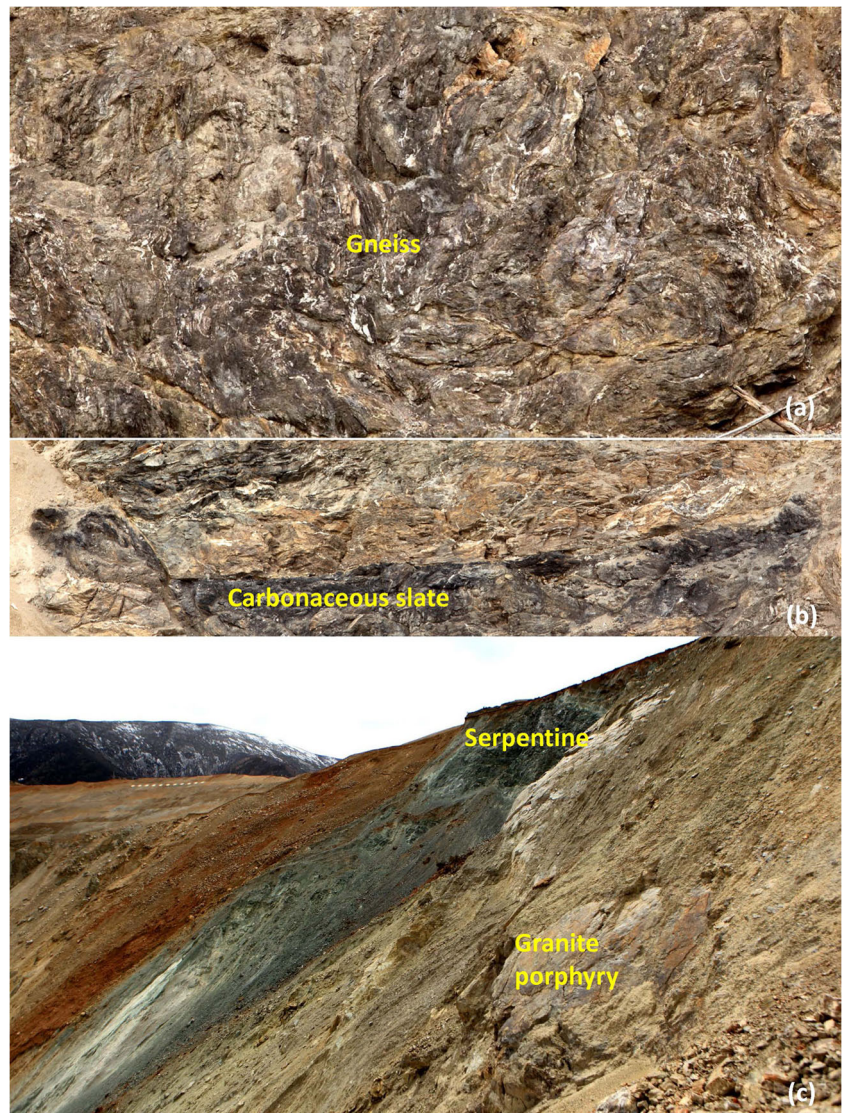
The source area of the “10.10” rockslide, converging at the toe and covering an area of $\sim 575 \times 10^3 \text{ m}^2$, is on the right bank as shown in Figs. 6 and 7a (outlined by dashed double-dot line). Outside the outline and near the toe of the slope, the zones of BZ1, BZ2, and UZ are not taken as part of the source, as they follow different mechanisms and contribute little volume to the source. Formation of the three zones will be discussed later.

After the slide, two newly formed platforms are left respectively at the elevations of $\sim 3500 \text{ m a.s.l.}$ and 3100 m a.s.l. , basically corresponding to the elevations of PF1 and PF2. Thus, the source area is further divided into three zones, i.e., the trailing zone TZ, the major sliding zone MZ, and the sliding-resistance zone SZ, based on their function in the sliding process. The three zones cover an area of $145 \times 10^3 \text{ m}^2$, $330 \times 10^3 \text{ m}^2$, and $100 \times 10^3 \text{ m}^2$, respectively, and the

corresponding volume is $4.6 \times 10^6 \text{ m}^3$, $13.3 \times 10^6 \text{ m}^3$, and $0.8 \times 10^6 \text{ m}^3$, with a total volume of $18.7 \times 10^6 \text{ m}^3$ and an average depth of 32 m.

The sliding-resistance zone is of tetrahedron shape and is composed of comparatively intact gneiss with no continuous and well-developed joints. Its failure plane is slicken sided with little debris left, demonstrating both high stress concentration and ability to resist sliding before the final failure. Based on the slickensides, the zone slides in the direction of $N65^\circ \text{ E}$ and the shear outlet is at the elevation of 2980 m a.s.l. Grass is well reserved below this elevation (Picture P1 in Fig. 7), where the zone is named as the undisturbed zone UZ, even though some debris can be found on its surface. Formation of the undisturbed zone suggests that the initiation of the slide bears a velocity and the debris in the deposition zones DZ1 and DZ2 was projected to the left bank. This inference makes sense as the shear outlet is 100 m higher above the normal water level of the river, and there exists a cove in the barrier

Fig. 4 Characteristics of bedrocks in the sliding area. See Fig. 6 for the locations



lake between UZ and DZ2 (Figs. 6 and 8). The initial velocity resulted from the abrupt energy release in the sliding-resistance zone, similar to strain-type rock burst in mechanism.

The major sliding zone MZ is a V-shaped groove controlled by two planes with attitudes of S30° E/38° (left side) and N62° W/35° (right side) respectively. The planes are not

Fig. 5 Cross section 1–1' of the “10.10” rockslide

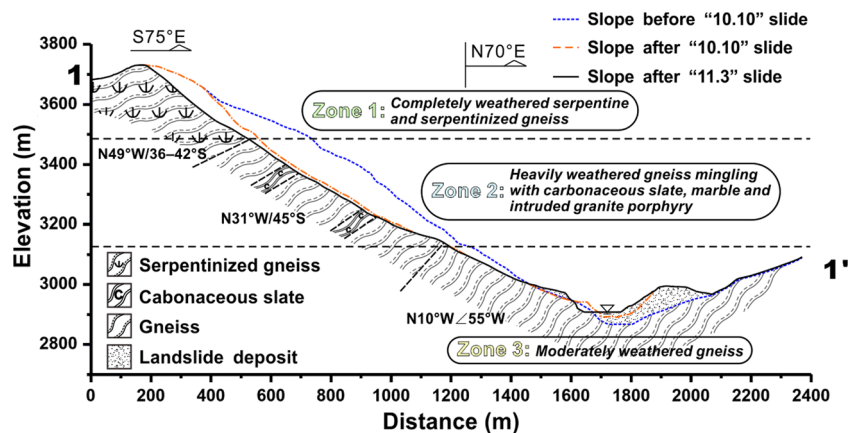
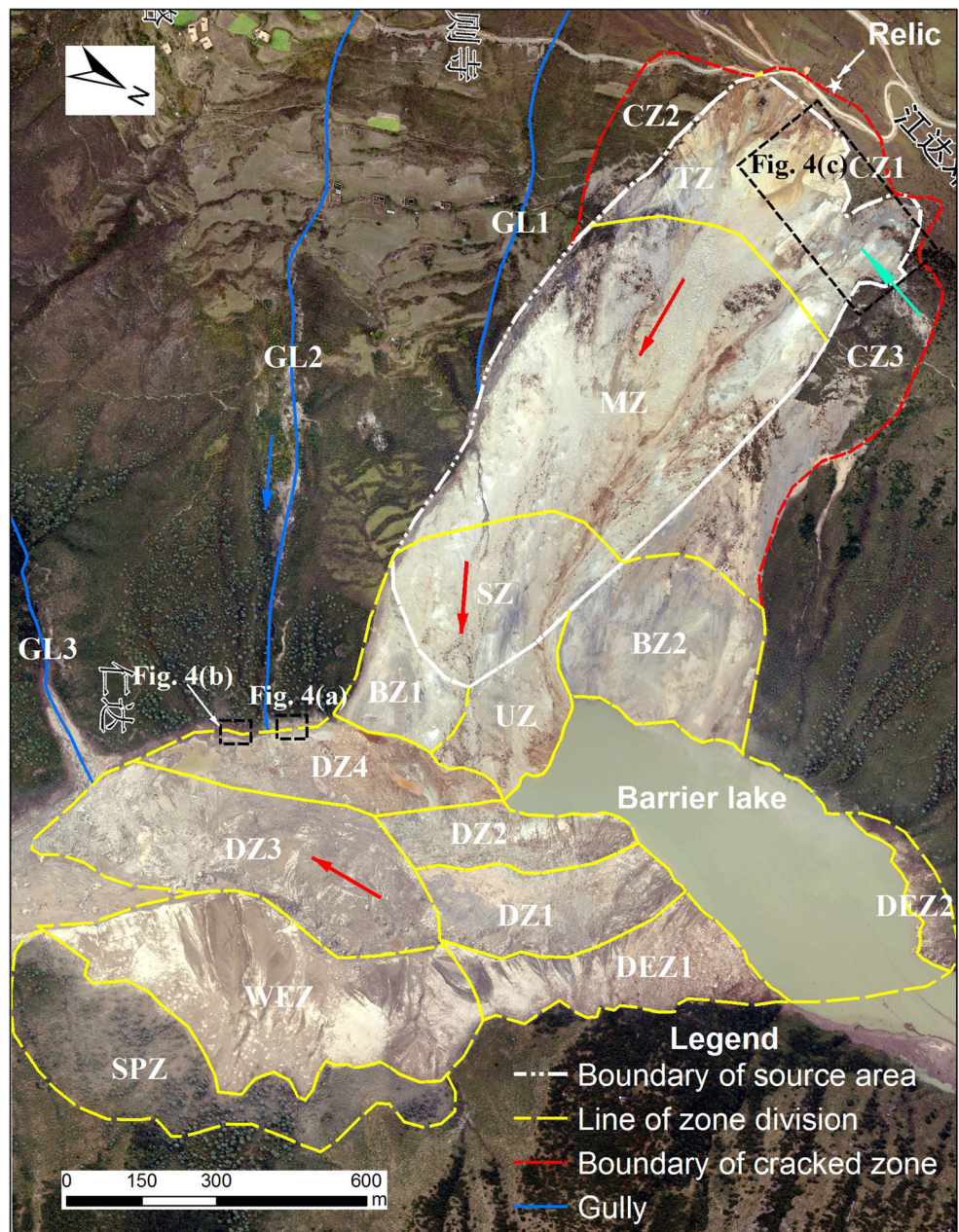


Fig. 6 Orthograph of the “10.10” rockslide



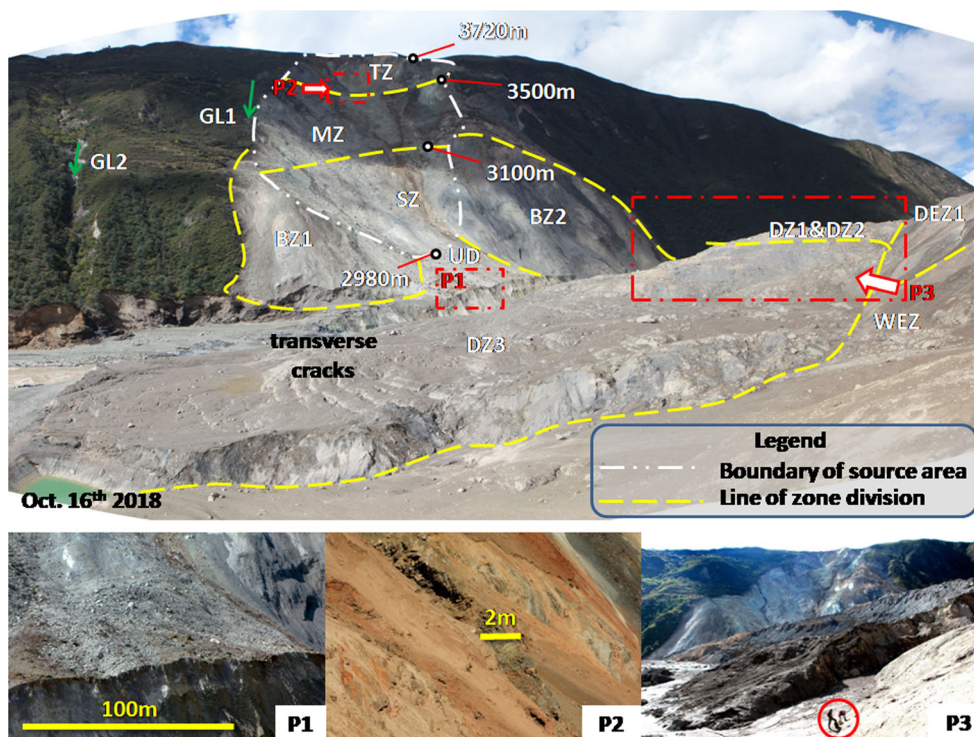
even, do not belong to any set of the 27 schistosity planes in the above section, and have not much slickenside left. So it is most likely that the planes get continuous during the process of the progressive slope deformation. The intersection of the two planes trends $S75^{\circ} E$ and plunges 24° to the SE. This direction is different from that in the sliding-resistance zone. The sliding left some debris in its groove, which was originated from the trailing zone TZ. The zone has the biggest area and volume in the three zones.

The trailing zone TZ is above the platform PF1 with a slope angle of 32° . It is mainly composed of completely weathered and altered gneiss and serpentine and some portions behave more like soil. However, some fractured rock lumps exist

locally, as can be evidenced in the main scarp (Picture P2 in Fig. 7), which is composed of heavily weathered and serpentized gneiss mingled with moderately weathered thin-layer granite porphyry and controls the behavior of TZ and the cracked zone CZ1.

Bedrock zones BZ1 and BZ2 are thus named as they are formed due to the surface erosion by the debris from the source area. They are not taken as part of the source area, as they contribute little volume to the whole landslide. BZ1 is located on PF3 (Fig. 3), and its surface erosion was made by debris partly from the major sliding zone MZ and mostly from the trailing zone TZ (Fig. 6). The surface of BZ2 is mainly eroded by the debris from the lower portion of the cracked

Fig. 7 Photograph of the “10.10” rockslide (mirror to west)



zone CZ3 (Fig. 6). Moreover, the lower portion of BZ2 was probably eroded by the high-speed waterjet, which will be discussed later. BZ1 and BZ2 cover areas of $\sim 45 \times 10^3 \text{ m}^2$ and $\sim 115 \times 10^3 \text{ m}^2$ respectively, and their existence may lead to the overestimation of the sliding volume.

Except for the small flow from Gully GL1, no obvious water was ever observed in the source area. It seems that underground water was not a major trigger of the slide.

Deposition area and landslide dam

Erosion on the left bank

Bank erosion is a typical feature of the “10.10” rockslide, and it mainly occurs on the left bank (Sichuan side) as shown in Figs. 6–8. The lower left bank consists in well-cemented colluvium, on which cypress, bush, and grass grow. After the “10.10” rockslide, an area of $285 \times 10^3 \text{ m}^2$ is badly eroded, with rarely any plant kelp. In terms of eroding agents, the eroded area can be divided into two types, i.e., debris-eroded zone DEZ1 and waterjet-eroded zone WEZ. For the debris-eroded zone, downslope slickensides can be witnessed and debris is kept locally (Picture P1 in Fig. 8). The debris can reach as high as 3050 m a.s.l. While for the waterjet-eroded area, only a thin layer of silt is kept along with locally scattered branches and barks of former cypress and bush (Picture P2 in Fig. 8). The waterjet-eroded area is located mainly to the downstream, and its highest point is 2985 m a.s.l. A third zone can also be seen outside the boundary of

WEZ, where leaves of cypress and bush are polluted by silt carried by the surged water mist and is thus named as silt-polluted zone, i.e., SPZ (Figs. 6 and 9).

Debris-eroded area and waterjet-eroded area can be also found on the right bank, i.e., DEZ2 and lower part of BZ2 in Figs. 6 and 7. Their formation will be discussed in the next section.

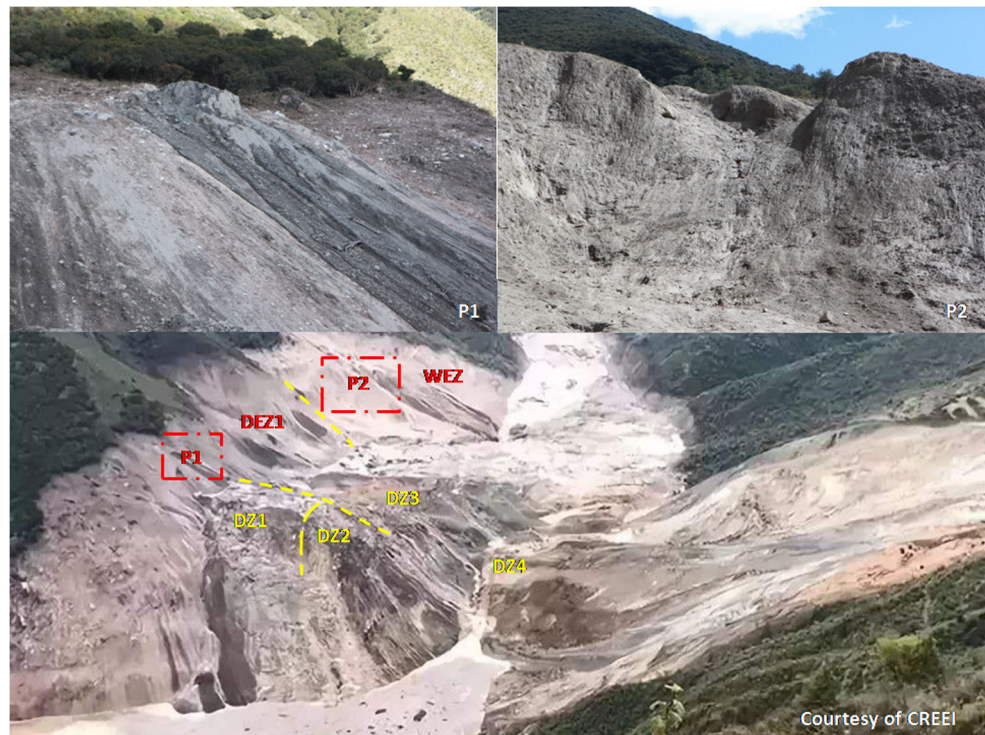
Landslide dam

The deposition area or the landslide dam is $\sim 1200 \text{ m}$ long along the river and $\sim 470 \text{ m}$ wide in the transverse direction, covering an area of $\sim 380 \times 10^3 \text{ m}^2$. The area was divided into four zones DZ1 to DZ4 (Fig. 6) mainly based on the lithology of debris.

For DZ1, moderately weathered gneiss boulders are common, suggesting their origin in the sliding-resistance zone SZ (Fig. 10). While for DZ2, it contains more fines of carbonaceous slate, which should be from the major sliding zone MZ. DZ1 and DZ2 constitute the left portion and also the highest portion of the landslide dam, and their highest point is 3005 m a.s.l.

DZ3 is a secondary landslide within landslide deposit of the “10.10” rockslide, as can be seen from the three scarps in its upstream and the transverse cracks in its downstream (Fig. 7 and its Picture P3). DZ3 should be part of DZ1 and DZ2 before further sliding, as can be evidenced by the boulders of gneiss and granite porphyry, and carboniferous-slate dominated fines in DZ3 (Fig. 11).

Fig. 8 Distribution of eroded areas on the left bank



DZ4 basically covers the former river bed. It is the right portion of the landslide dam, but its elevation is much lower than that of DZ1, constituting the bealock of the landslide dam and having an elevation of 2931.4 m a.s.l. Furthermore, debris in DZ4 contains lots of fines (Fig. 12), which are mainly composed of completely weathered serpentine, intermingled with serpentized gneiss blocks, indicating its origin in the trailing zone TZ. Due to its low height and erodibility, the

overtopping failure of the natural dam occurred at DZ4 on Oct. 13, 2018, and a sluice channel (Fig. 12) was quickly formed by dam-beaching flood. Not much debris was left in the zone after the flood.

The sluice channel is ~1000 m long, ~80 m wide at base, and ~152 m wide at the right wall crest. The heights of the left and right walls are ~76 m and ~52 m, respectively. The right wall is composed of the former colluvium, while the left wall

Fig. 9 Cypress and bush polluted by silt in zone SPZ. See Fig. 6 for the location



Fig. 10 Characteristics of deposition zone DZ1 and debris-eroded zone DEZ2



is of landslide deposit. The left wall is quite stable although some longitudinal cracks can be found behind its crest. No collapse was ever witnessed during field work.

In general, the debris in the dam is quite fractured but compact. It is not difficult to walk on the surface of DZ3 during our first visit on October 16, 2018, even it was badly flushed by surged water.

Mechanism

The slope deformation was firstly documented by Chengdu Engineering Corporation Limited of Power China, the design agency of the Yebatan Hydropower Station in 2009 during the geological investigation of its reservoir area; then in 2011, all residents on the slope are relocated by local government. The

slope deformation has been traced back to 1966 by Fan et al. (2019) based on historical remote sensing images.

Other features of the slide can be summarized as follows. First, it is a high-speed landslide with a high position and a high shear outlet. The slope is over 800 m above the riverbed; its shear outlet is 100 m above the riverbed, and the landslide deposit climbed up the left bank for ~70 m higher than the shear outlet elevation of the “10.10” Baige rockslide. Secondly, the slide started up with an initial velocity. The landslide body did not slide into the riverbed; instead, it hit the left bank directly, as can be evidenced by the cove of the barrier lake and the well-kept grass below the shear outlet. Thirdly, it is a new rockslide and is not the reactivation of an old one. The slope shows little features of an old slide, but new slickensides and shear failure features are obvious in the sliding-resistance zone.

Fig. 11 Debris features in the deposition zone DZ3



Fig. 12 Photograph of the sluice channel and its left bank debris



As there is no evidence that either earthquake or rainfall induced the landslide, it is more likely that the “10.10” rockslide is the result of geomorphological evolution of the slope and its major cause is gravitational slope deformation. Such a hillslope movement gradually develops, and the process can be depicted as follows. First, the weathering process of the serpentine and the serpentized gneiss in the trailing zone leads to its strength reduction. Once the strength is not sufficient to maintain its slope stability, the upper slope will deform and exert a pressure in the major sliding zone; then under the above pressure, the non-preferential joints in the major sliding zone get interconnected progressively, producing the two controlling structural planes in the major sliding zone and reducing their shear strength. The existence of the weak rock, i.e., carbonaceous slate in the zone would facilitate the above process; and finally, the stresses in the sliding resistance zone gradually concentrates when the above two planes become more and more continuous. When the stress concentration dominates the peak strength of its rocks, the sliding resistance zone fails suddenly, resulting in the high speed sliding of the entire slope. In general, the landslide is a gravitational failure, and historical earthquake and rainfall may accelerate the failure process during the slow deformation.

Sliding process

The deformation initiated from up to down; however, the actual sliding process is just converse. Based on the features in the deposition area and the eroded left bank, the kinematic process of the slide can be divided into six steps (Fig. 13).

Step 1. Startup of the major sliding and sliding resistance zones (Fig. 13a)

The sliding-resistance zone was firstly sheared off, and the sudden energy released from the brittle failure makes the sliding-resistance zone SZ and the major sliding zone MZ slip out with an initial speed. The movement was initially towards the direction of $N65^{\circ} E$; then the moving direction changed to $S75^{\circ} E$ due to the inertia of the major sliding zone, which eroded PF3, leading to the broadening of the shear outlet and the exposing of the bedrock zone BZ1.

Step 2. Sliding initiation of the trailing zone (Fig. 13b)

By losing the support from the major sliding zone, the trailing zone began to collapse and gravitationally moved downward along the direction of $S75^{\circ} E$. As the trailing zone is mainly composed of completely weathered rocks, its sliding bears no initial velocity. That is, its velocity is much lower than that of the major sliding and sliding-resistance zones, so its deposition is at the toe of the slope (DZ4). The debris slid directly, overtopping the bedrock zone BZ1 and making it further eroded.

Step 3. Formation of debris-eroded zone DEZ1 and DEZ2 (Fig. 13c)

After startup, the major and sliding-resistance zones were projected at an initial speed that then accelerated under gravity. Finally, the landslide body bumped the left bank (Sichuan side) at high speed and run up the left bank for ~ 70 m. The bumping leads to the further fragmentation and side-spreading of the debris, resulting in the debris-eroded zone DEZ1 (Fig. 6). Due to the convex shape of the left bank, partial debris moves upstream to the right bank (Tibet side), forming a small debris-eroded zone DEZ2 (Figs. 6 and 10). When the debris reached the highest point (3050 m a.s.l.) on the left bank, it

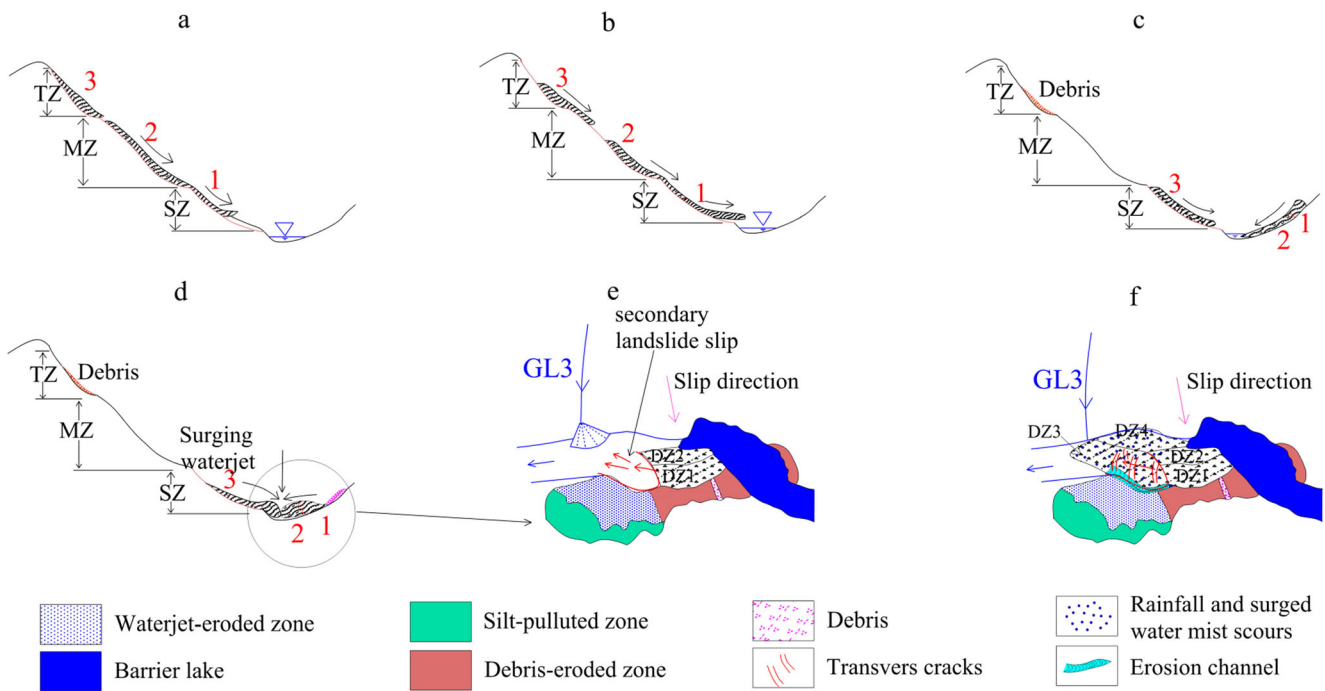


Fig. 13 Kinematic process of the “10.10” rockslide

began to slip downward under gravity, leaving some debris on relatively gentle steps and resulting strips (similar to slickensides) along the left bank (Fig. 8).

Step 4. Debris collision and surging waterjet and mist

As the trailing zone moved downslope to the river bed, it collided with the debris just returned from the left bank. The collision carried the debris downward and jammed the river water, triggering high-speed waterjet and surging water mist. The speed of the waterjet should be sufficiently high as it cleared up all the surface soil and plants in a zone on the left bank, i.e., the waterjet-eroded zone WEZ. It can be rationally inferred that the lower part of the bedrock zone BZ2 on the right bank should also be cleared up by the waterjet. However, the evidence is not as outstanding as that on the left bank. The comparatively low speed of the trailing zone and the collision deposited its debris mainly on the west side of the deposition area but just on the river bed. It is most likely that the deposition zone DZ4 extends further downstream due to river flow and the fluidization of its debris, and the zone is finally confined downstream by an alluvium fan at the estuary of gully GL3. As to the surged water mist, it disperses silt on the plant leaves in the silt-polluted zone SPZ, adjacent to the waterjet-eroded zone WEZ.

Step 5. Secondary landslide of the landslide dam

As the shear outlet converges, the debris from zones MZ and SZ was first deposited in the zones DZ1 and DZ2. The

highly concentrated debris accumulation formed a landslide dam to the left bank. Due to the changing sliding direction, the debris is coarser in the upstream slope of the dam, while the debris is more fine-grained in the downstream slope. That is, the debris from SZ is deposited toward upstream and that from MZ toward the downstream. Both slopes are unstable due to highly concentrated accumulation and high speed bumping. So the upstream slope failed and formed the debris-eroded zone DEZ2 on the right bank (Fig. 10); and the downstream slope slipped, leading to a secondary landslide zone DZ3. The secondary slip was then blocked by the aforementioned fan on the right bank, bringing about the generation of the transverse cracks in Fig. 7.

Step 6. Surface scouring in the deposition area

The surface in the deposition area was scoured by both rainfall from the surged water mist and the flow running down from the WEZ. In general, DZ1 and DZ2 were only slightly scoured, whereas the scouring on the downstream zones DZ3 and DZ4 was more severe due to water confluence from higher sites (Fig. 7).

“11.3” rockslide

Source area

After the “10.10” rockslide, there exist three cracked zones CZ1, CZ2, and CZ3 beyond its boundary, constituting

potential portions for a further sliding (Figs. 6 and 14). The area of CZ1, CZ2, and CZ3 is $52 \times 10^3 \text{ m}^2$, $66 \times 10^3 \text{ m}^2$, and $130 \times 10^3 \text{ m}^2$, respectively, and the estimated volume is $4.6 \times 10^6 \text{ m}^3$, $1.5 \times 10^6 \text{ m}^3$, and $2.6 \times 10^6 \text{ m}^3$, respectively.

CZ2 is similar to CZ1, and there exist fractured rock lumps at its toe (above 3500 m a.s.l., Picture P1 in Fig. 14). But the slope in CZ2 is much gentler than the main scarp in CZ1. CZ3 actually comprises two small sliding blocks overlain by shallow overburdens (Picture P2 in Fig. 14). The first one CD3-1 is located above the platform PF1, and the second one is located between PF1 and PF2. Both CD3-1 and CD3-2 have been deforming rather fast, and their depths are confined in-depth, respectively, by intruded granite porphyry and moderately weathered gneiss. Majority of CZ3 deforms in the down-slope direction, demonstrating an independent deformation. The debris, collapsed at its toe, eroded the surface of the lower slope, forming the bedrock zone BZ2. Only the portion adjacent to the source area of the “10.10” rockslide deforms towards the groove.

During field investigation, no collapse ever occurred along the boundary of the “10.10” rockslide. It is so at the main scarp, even though it is quite steep and high. Deformation of the cracked zones was monitored by both crackmeters and Global Navigation Satellite System (GNSS) during emergency response and results indicated that the deformation tends to cease and the cracked zones are not prone to a landslide (Fig. 15). Unfortunately, on Nov. 3, 2018, part of the CZ1 and CZ3-1 (Fig. 14) slid down and the Jinsha River was dammed again as shown in Fig. 16.

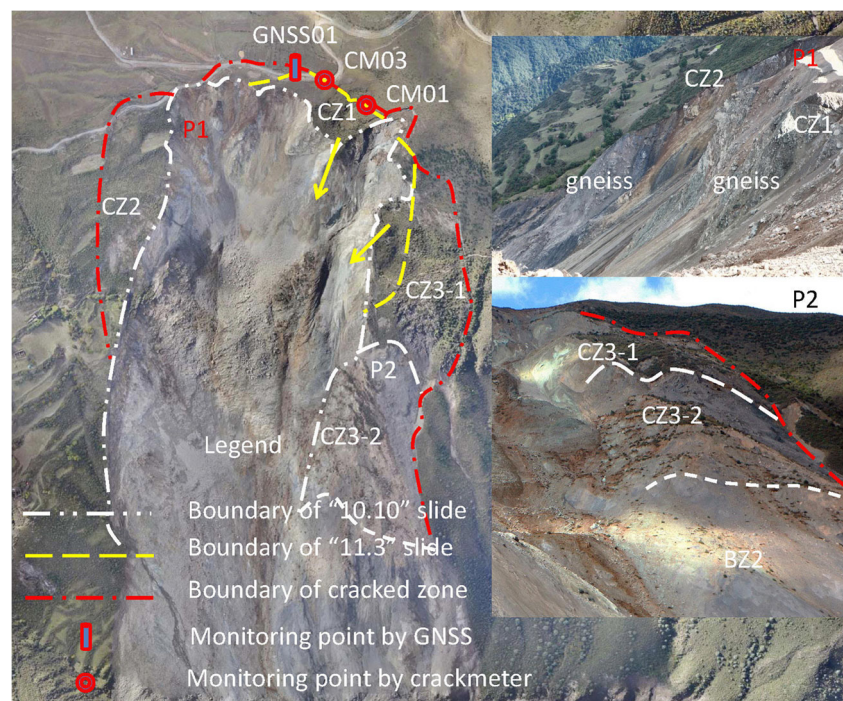
The slide occurred at around 15:40. The sliding portion in CZ1 and CZ3-1 covers an area of $30 \times 10^3 \text{ m}^2$ and $19 \times 10^3 \text{ m}^2$, respectively, and the calculated volume is around $2.8 \times 10^6 \text{ m}^3$, based on the DEM before and after the “11.3” rockslide. Adding the entrained debris in the groove, total volume can attain $6.3 \times 10^6 \text{ m}^3$.

Deposition area

The deposition area is mainly distributed on the sluice channel of the “10.10” rockslide (Fig. 16), due to the relatively lower speed and smaller volume of the slide. The area is quite similar to DZ4 of the “10.10” rockslide, but the elevation of the new dam is much higher. The bealock of the new landslide dam is still at the right side, and its elevation can attain as high as 2967 m, ~36 m higher than that of the “10.10” rockslide. As a disaster reduction measure, an artificial channel was excavated, starting at night on Nov. 8, 2018, and ending at 11:00 on Nov. 11, 2018. The artificial channel follows basically the sluice channel of the “10.10” rockslide, and its bottom elevation is 2952.5 m. Flood passed through the channel at approximately 10:50 on Nov. 12, 2018, and the river’s flow rate returned to a normal value of $700 \text{ m}^3/\text{s}$ at 7:40 on Nov. 14, 2018. A new sluice channel was formed as shown in Fig. 17.

Waterjet is also surged by the debris, but its projected distance is not as long as the “10.10” rockslide (Fig. 16). The debris was fluidized too, flowed downstream, and was finally intercepted by the alluvium fan at the estuary of gully GL3. As the source is above the platform PF1 belonging to the

Fig. 14 Distribution of the cracked zones and the boundary of the “11.3” rockslide



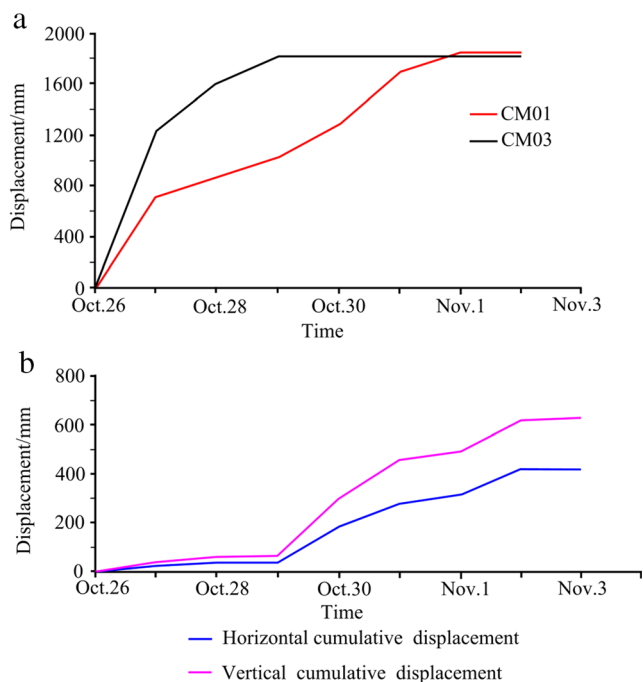


Fig. 15 Monitored displacements by GNSS and crackmeters before the “11.3” rockslide. See Fig. 14 for the location of the instruments

completely weathered Zone 1, the debris is basically fine-grained gneiss and serpentine. However, a huge boulder of granite porphyry exists locally (Picture P1 in Fig. 17), which is originated from the toe of CZ3-1. This may suggest that the sliding of CZ1 and CZ3-1 did not occur simultaneously and the debris from CZ3-1 lags behind that from CZ1, as can be evidenced by the rock types in the deposition area. The sliding direction of $\sim S75^\circ E$ corresponds to the route of the major sliding zone; as a result, the surface of bedrock zone BZ1 was further eroded and the failure outlet is further broadened.

Fig. 16 Photograph of the landslide dam produced by the “11.3” rockslide



Mechanism

The mechanism of the “11.3” slide can be shown in Fig. 18a. The failure mode was first proposed by Min et al. 2005. In the failure mode, the fractured rock lump behaves as a retaining wall and cannot be easily sheared off. But due to its existence and the valley ward deformation of the potential sliding mass in the cracked zones induced by the “10.10” rockslide, the sliding mass may disintegrate into two blocks (Blocks 1 and 2 in Fig. 18a). Block 1 may subside under gravity, acting as a wedge and making Block 2 revolve. The gradual revolving of Block 2 will reduce both the compressive stress and the shear strength at the toe of Block 2, making the rock lump (Fig. 18a) more prone to a failure.

The failure in the cracked zone CZ1 follows this mode, as can be evidenced by the ground subsidence (Fig. 18b) just behind the crest of the main scarp. This type of failure mode may be named as wedge cleaving effect and can easily trigger a landslide without much prior deformation. As to the failure in CZ3-1, debris erosion at its toe is the major trigger.

Discussions

Deformation history

In a discussion with Sakya living Buddha of Gongze Monastery on the building relic sited behind the main scarp (Figs. 3 and 6), he said it was left by the former Tangxia Monastery, which was moved to adjacent Gongjue County around two hundred to three hundred years ago. Though the authors tried in vain to find any official document related to the relocation of the monastery, it is still believed that the

Fig. 17 Sluice channel after dam breaching of the “11.3” rockslide dam



relocation is closely related to the slope deformation. From the microtopography adjacent to the sliding area, berms are quite common and most of the sliding-induced cracks appear along the berms (Pictures P1 to P3 in Fig. 19). So the berms should be naturally formed during the long-term toppling deformation of the slope. Formation of the berms can be interpreted in Fig. 20. That is, the deformation history of the slope is quite long and may be traced back to prehistoric time, as can also be evidenced by the weathering degree of gneiss beside the berms (Picture P4 in Fig. 19). The closer to the sliding area, the heavier the weathering degree. In general, the slides are the result of long-term geomorphological evolution due to river incision.

Landslide speed

Based on the paper by Scheidegger (1973), the average coefficient of friction f is 0.36 for the “10.10” rockslide, as defined

by the angle of repose. The value is lower than the reversed one of 0.47 by Zhang et al. (2019b). As the slide starts with an initial velocity, the value 0.47 seems more rational and is thus used for the velocity estimation below.

With reference to the schematic view in Fig. 21, the upclimbing height is used to estimate the sliding velocity. As suggested by Scheidegger (1973), the velocity can be written as

$$u = \sqrt{2gH \left(1 + \frac{f}{\tan\alpha} \right)} \quad (1)$$

g is gravity acceleration, 9.8 m/s^2 , H is the upclimbing height of the sliding debris in meter, and α is slope angle.

Two extreme trajectories are assumed. The first one is along the route O-a-b-O'-c, corresponding to the status that the slide starts at rest and the upclimbed height is 170 m. A velocity of $u_a = 81 \text{ m/s}$ is then got. The second route O-O'-c assumes the slide is projected from the shear outlet O to the

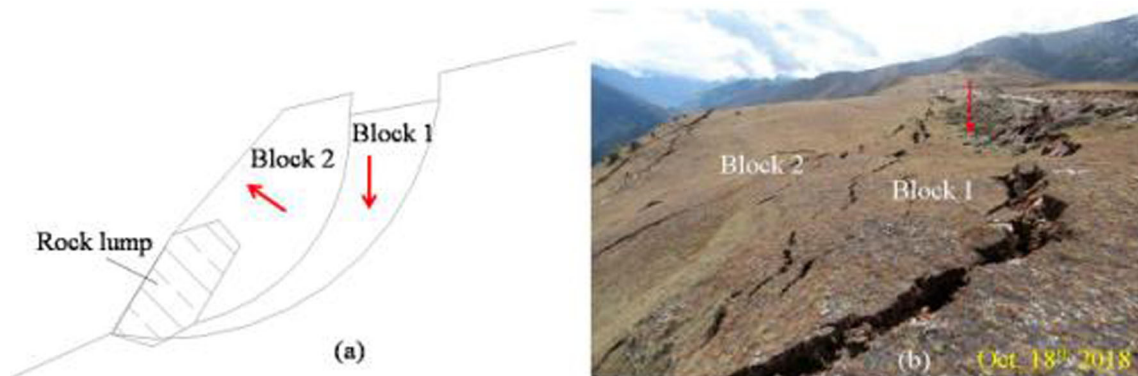


Fig. 18 Schematic failure model and photograph of the “11.3” rockslide

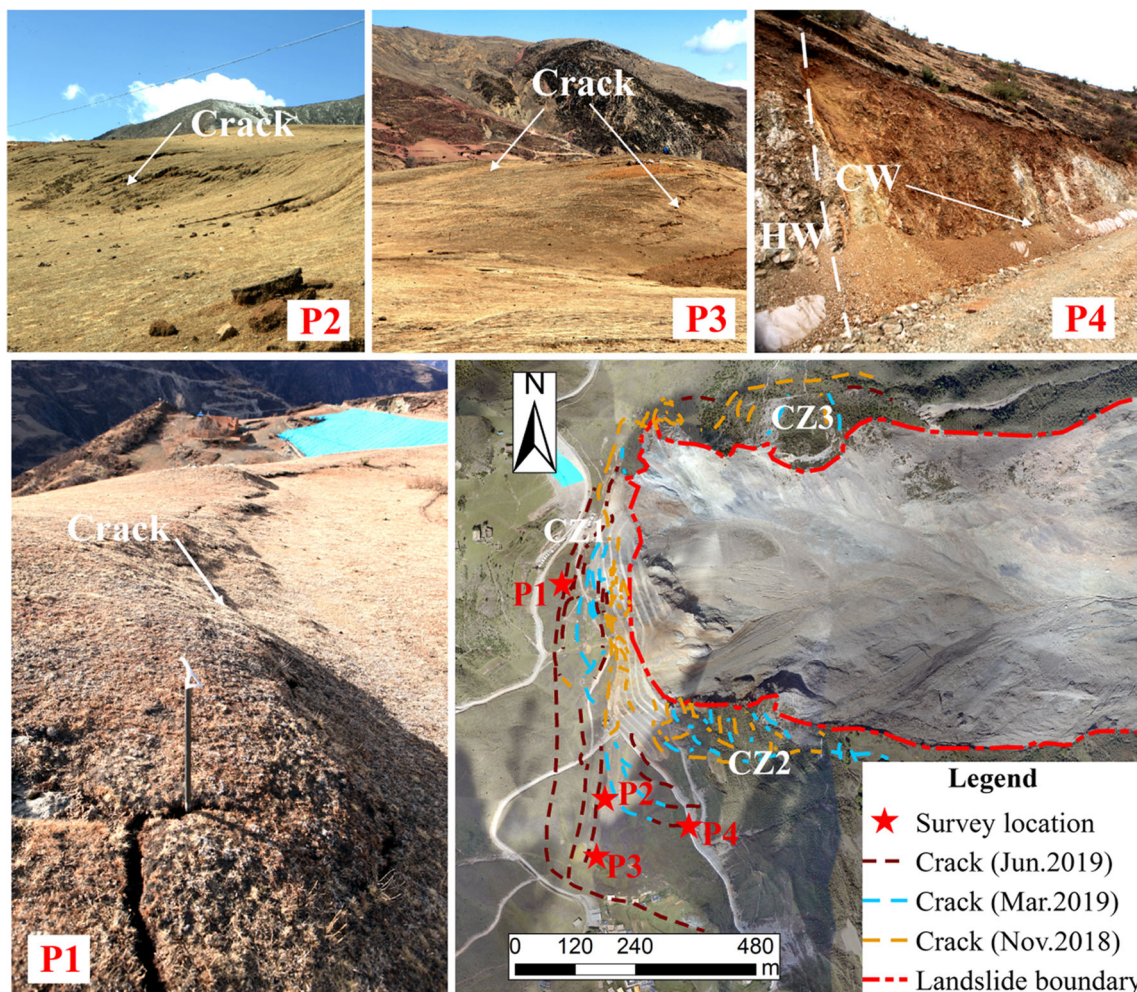


Fig. 19 Development of cracks and their relation with microtopography

Fig. 20 Schematic view for the formation of the berms

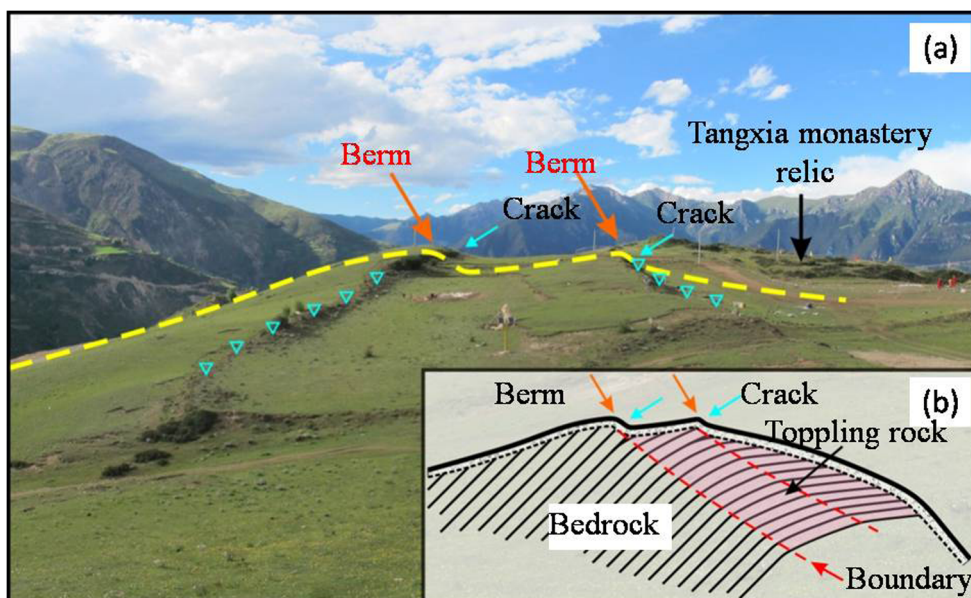
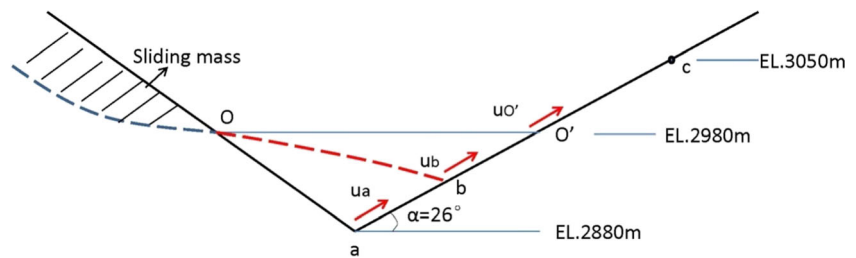


Fig. 21 Schematic view for velocity estimation



point O' , which is at the same elevation of the shear outlet O on the opposite bank. The upclimbing height is 70 m, and the estimated velocity is $u_{O'} = 52$ m/s. The true route is along O - b - O' - c , lying between points a and O' , so the velocity of u_b should be between 52 m/s and 81 m/s.

Zhang et al. (2019b) divides the sliding process into three stages, and each stage has a nearly constant sliding direction. In the authors' opinion, the first stage should correspond to Steps 1–3 depicted in Section 3.4 when the sliding direction is around $N65^\circ E$; the second stage reflects the reversed movement of the debris from the left bank in Step 4, and the sliding direction is $S60^\circ W$, while the third stage is the second landslide of the landslide dam and its direction is around $S20^\circ E$. This inference makes sense as the directions comply with the depiction in the literature. So the time of 22 s for the first stage can be used to refine the velocity estimation. The horizontal distance between points O and c is 670 m; an averaged horizontal velocity of 30 m/s is obtained. The horizontal velocity at point b can be roughly estimated as 60 m/s omitting the time consumed between points O and b , which is much smaller than that between points b and c . u_b is finally estimated as $60/\cos 26^\circ = 67$ m/s, and point b is at around the elevation of 2940 m.

Future impacts

After the “11.3” rockslide, a series of new cracks, as shown in Fig. 19, generated behind CZ1 and CZ2 and the generation sustains until June 2019, when all the cracked zones have reached an area of 258×10^3 m² and the estimated volume is $\sim 9 \times 10^6$ m³.

Collapse frequently occurs in small scale from the main scarp during our field investigation. What concerns us most is the future development of the cracking zones, and it seems that the risk of another landslide damming event may happen sooner or later.

In order to reduce the risk, two measures were conducted in the year 2019 besides deformation monitoring. First, soil of 0.56×10^6 m³ was removed from the crest of the main scarp in an effort to lower down the stress concentration at its toe. Secondly, debris of 2.45×10^6 m³ was excavated from the landslide dam and moved to its downstream and to the left bank, so more space is left at the former dam site to reduce the dam height by a potential landslide.

The first measure is effective to a certain extent as the deformation rate slows down in the end of 2019. However, the risk has not been eliminated yet as the deformation continues. In the short term, the second measure may reduce the impacts of a potential damming event on the downstream facilities, including the Yebatan Hydropower Station being under construction. In the long run, great impacts may lie in the feasibility of the upstream hydropower station planned and sited in Boluo Town, as the present river water level is still around 10 meters above the normal one and another landslide event may occur in the near future. To the impacts, no better solution is ever found by now.

Conclusions

Based on the field investigation from Oct. 2018 to Apr. 2020, the geology is described; the mechanism and sliding process are analyzed for the two Baige landslides. Major conclusions can be summarized as follows:

- (1) The two Baige landslides occurred in the suture belt of the Jinsha River. Due to periodically tectonic movement, the rocks in the sliding area are composed of tectonic mélange slices of mainly gneiss intermingled with carboniferous slate and marble and with intruded serpentine and granite porphyry. Even though with the tectonic background, the gneiss generally bears a schistosity plane with an averaged attitude of $N47^\circ W/47^\circ$, dipping into the slope.
- (2) The “10.10” landslide is the result of long-term geomorphological evolution of the bank slope due to river incision. No preferential joints exist in the slope, but alteration and weathering play important roles in the slide occurrence. Rainfall and earthquakes may accelerate the slope deformation.
- (3) The “10.10” landslide is high-speed wedge-like slope failure with a high position and a high-shear outlet. Its sliding and deposition process demonstrate some special features as initial speed, collision between debris, surging waterjet, and second slipping.
- (4) The whole process of the “10.10” landslide can be divided into 6 steps, i.e., startup of the major sliding and sliding-resistance zones, sliding initiation of the trailing

zone, formation of debris-eroded zones, collision of debris and triggering waterjet and mist, secondary slip of the landslide dam, and surface flush in the deposition area. The estimated speed may reach as high as 67 m/s.

- (5) The “11.3” landslide follows a different mode from the “10.10” landslide, named wedge cleaving effect.
- (6) The cracked zones still have the risk to constitute a potential landslide that might dam the river again.

Acknowledgements Thanks should be given to our partners from Sichuan Huadi Construction Engineering Limited, Tibetan Geoenvironmental Monitoring Center, Shenzhen Baidou Information Technology Corporation Limited, and 915 Geological Investigation Corporation Limited.

Author contribution All the authors participated in the field work and related discussion, Chen and Deng prepared the draft of this manuscript, Gao and Zhao helped to provide most of drawings, and Zhao also helped to polish the draft.

Funding This study was financially supported by National Key R&D Program of China (2018YFC15050006) and the Second Tibetan Plateau Scientific Expedition and Research Program (2019QZKK0905). The support from the Natural Resources Bureau of Changdu City and Tibetan Autonomous Region, Sichuan Bureau of Surveying, Mapping and Geoinformation, China Renewable Energy Engineering Institute (CREEI), is greatly appreciated.

Data availability All data, models, and code generated or used during the study appear in the submitted article.

Code availability Not applicable.

Declarations

Competing interests The authors declare that they have no known competing financial interests or personal relationships that could have appeared to influence the work reported in this paper.

References

- Chen Y, Zhou F, Feng Y, Xia Y (1992) Breach of a naturally embanked dam on Yalong river. *Can J Civ Eng* 19:811–818
- Chen J, Dai F, Lv T, Cui Z (2013) Holocene landslide-dammed lake deposits in the Upper Jinsha River, SE Tibetan Plateau and their ages. *Quat Int* 298:107–113
- Chen J, Zhou W, Cui Z, Li W, Wu S, Ma J (2018) Formation process of a large paleolandslide-dammed lake at Xuelongnang in the upper Jinsha River, SE Tibetan Plateau: constraints from OSL and C-14 dating. *Landslides* 15:2399–2412
- Chen J, Cui Z, Liu C, Zhou W, Chen R (2019) Meso/micro-texture analysis of the landslide-dam outburst sediments in the Upper Jinsha River, SE Tibetan Plateau. *Geol Croatica* 72:81–91
- Chen Z, Zhang Q, Chen S, Wang L, Zhou X (2020) Evaluation of barrier lake breach floods: insights from recent case studies in China. *Wiley Interdiscip Rev-Water* 7. <https://doi.org/10.1002/wat2.1408>
- Dai F, Lee C, Deng J, Tham L (2005) The 1786 earthquake-triggered landslide dam and subsequent dam-break flood on the Dadu River, southwestern China. *Geomorphology* 65:205–221
- Deng H, Wu L, Huang R, Guo X, He Q (2017) Formation of the Siwani ancient landslide in the Dadu River, China. *Landslides* 14:385–394
- Fan X, Xu Q, Alonso-Rodriguez A, Subramanian S, Li W, Zheng G, Dong X, Huang R (2019) Successive landsliding and damming of the Jinsha River in eastern Tibet, China: prime investigation, early warning, and emergency response. *Landslides* 16:1003–1020
- Fan X, Yang F, Subramanian SS, Xu Q, Feng Z, Mavrouli O, Peng M, Ouyang C, Jansen J, Huang R (2020) Prediction of a multi-hazard chain by an integrated numerical simulation approach: the Baige landslide, Jinsha River, China. *Landslides* 17:147–164
- Li H, Qi S, Chen H, Liao H, Cui Y, Zhou J (2019) Mass movement and formation process analysis of the two sequential landslide dam events in Jinsha River, Southwest China. *Landslides* 16:2247–2258
- Li M, Zhang L, Ding C, Li W, Luo H, Liao M, Xu Q (2020a) Retrieval of historical surface displacements of the Baige landslide from time-series SAR observations for retrospective analysis of the collapse event. *Remote Sens Environ* 240. <https://doi.org/10.1016/j.rse.2020.111695>
- Li Y, Jiao Q, Hu X, Li Z, Li B, Zhang J, Jiang W, Luo Y, Li Q, Ba R (2020b) Detecting the slope movement after the 2018 Baige Landslides based on ground-based and space-borne radar observations. *Int J Appl Earth Obs Geoinf* 84. <https://doi.org/10.1016/j.jag.2019.101949>
- Liang G, Wang Z, Zhang G, Wu L (2019) Two huge landslides that took place in quick succession within a month at the same location of Jinsha River. *Landslides* 16:1059–1062
- Liu X, Zhao C, Zhang Q, Lu Z, Li Z (2020) Deformation of the Baige landslide, Tibet, China, revealed through the integration of cross-platform ALOS/PALSAR-1 and ALOS/PALSAR-2 SAR observations. *Geophys Res Lett* 47. <https://doi.org/10.1029/2019gl086142>
- Ma J, Chen J, Cui Z, Zhou W, Liu C, Guo P, Shi Q (2018) Sedimentary evidence of outburst deposits induced by the Diexi paleo landslide-dammed lake of the upper Minjiang River in China. *Quat Int* 464: 460–481
- Min H, Deng J, Wei J, Zhang Q, Zou J, Zhou Z (2005) Slope safety control during mining below a landslide. *Sci China Ser E* 48(Supp):47–52
- Ouyang C, An H, Zhou S, Wang Z, Su P, Wang D, Cheng D, She J (2019) Insights from the failure and dynamic characteristics of two sequential landslides at Baige village along the Jinsha River, China. *Landslides* 16:1397–1414
- Scheidegger A (1973) On the prediction of the reach and velocity of catastrophic landslides. *Rock Mech* 5(4):231–236
- Tian S, Chen N, Wu H, Yang C, Zhong Z, Rahmanet M (2020) New insights into the occurrence of the Baige landslide along the Jinsha River in Tibet. *Landslides* 18:1207–1216
- Wang P, Chen J, Dai F, Long W, Xu C, Sun J, Cui Z (2014) Chronology of relict lake deposits around the Suwalongpaleolandslide in the upper Jinsha River, SE Tibetan Plateau: Implications to Holocene tectonic perturbations. *Geomorphology* 217:193–203
- Wang W, Yin Y, Zhu S, Wang L, Zhang N, Zhao R (2019a) Investigation and numerical modeling of the overloading-induced catastrophic rockslide avalanche in Baige, Tibet, China. *Bull Eng Geol Environ* 79:1765–1779
- Wang Y, Wu LZ, Gu J (2019b) Process analysis of the Moxi earthquake-induced Lantianwan landslide in the Dadu River, China. *Bull Eng Geol Environ* 78:4731–4742
- Wei Y, Wang X, Sheng M, Zhou Z, Yuan Y (2015) Reproduction of the sedimentary disturbance phenomenon of the Diexi ancient landslide-dammed lake under earthquake. *J Mt Sci* 12:1181–1188
- Wu Y, Niu R, Lu Z (2019) A fast monitor and real time early warning system for landslides in the Baige landslide damming event, Tibet.

- China Nat Hazards Earth Syst Sci Discuss. <https://doi.org/10.5194/nhess-2019-48>
- Yang W, Wang Y, Wang Y, Ma C, Ma Y (2019) Retrospective deformation of the Baige landslide using optical remote sensing images. *Landslides* 17:659–668
- Zhang Y, Zhao X, Lan H, Xiong T (2011) A Pleistocene landslide-dammed lake, Jinsha River, Yunnan, China. *Quat Int* 233:72–80
- Zhang L, Xiao T, He J, Chen C (2019a) Erosion-based analysis of breaching of Baige landslide dams on the Jinsha River, China, in 2018. *Landslides* 16:1965–1979
- Zhang Z, He S, Liu W, Liang H, Yan S, Deng Y, Bai X, Chen Z (2019b) Source characteristics and dynamics of the October 2018 Baige landslide revealed by broadband seismograms. *Landslides* 16:777–785
- Zhao S, Chigira M, Wu X (2019) Gigantic rockslides induced by fluvial incision in the Diexi area along the eastern margin of the Tibetan Plateau. *Geomorphology* 338:27–42